Diameter Selective Growth of Vertically Aligned Single Walled Carbon Nanotubes and Study on Their Growth Mechanism

Myung Gwan Hahm,[†] Young-Kyun Kwon,[‡] Eunah Lee,[§] Chi Won Ahn,[||] and Yung Joon Jung*,[†]

Department of Mechanical and Industrial Engineering, Northeastern University, Boston, Massachusetts 02115, Department of Physics and Research Institute for Basic Sciences, Kyung Hee University, Seoul, 130-701, Korea, Molecular and Microanalysis Division, HORIBA Jobin Yvon Inc., Edison, New Jersey 08820, and New Technology & Analysis Division, National Nanofab Center, Daejon, 305-806, Korea

Received: August 18, 2008; Revised Manuscript Received: September 18, 2008

Diameter controlled vertically aligned single walled carbon nanotubes (VA-SWNTs) were synthesized by controlling flow rate of carbon source and dimension of catalyst nanoparticles. The large scale structural analysis demonstrating spatial distribution of SWNT diameters was conducted by a newly developed Raman Radial Breathing Mode (RBM) mapping technique. Also we investigated the fundamental mechanism of diameter selective growth of SWNTs during the CVD process through computational modeling. Our experimental and computational studies show that a lower flow rate of carbon source makes a smaller nucleation site for a SWNT resulting in a smaller diameter formation. On the other hand, a higher flow rate of carbon source forms a larger nucleation site growing a SWNT with the larger diameter.

Introduction

The most promising applications of single walled carbon nanotubes (SWNTs) are their use in nanoelectronics such as field effect transistors, interconnects, and nanosensors by virtue of their specific electronic structures (either metallic or semiconducting), transport properties, and unique one-dimensional nanostructure.[1−3] For the synthesis of SWNTs, chemical vapor deposition (CVD) methods are becoming a strong manufacturing route due to the ability of producing SWNTs on a large-scale and controlling their structure more easily compared to other synthesis methods.[4] Many experimental studies[5−8] have been conducted toward investigating the growth mechanism of SWNTs in order to produce SWNTs with desired structures and properties in a CVD process. Especially considering the unique electronic properties of SWNTs arising from their structural parameters such as diameter and chirality, the large-scale synthesis of SWNTs with predetermined diameter and chirality is one of the biggest challenges that needs to be solved for the application of SWNTs in future nanoscale-electronic devices.

In a thermal CVD process, usually metallic nanoparticles are used as catalyst for the growth of SWNTs on various substrates. Most times one catalyst nanoparticle nucleates one SWNT and the diameter of SWNT is approximately correlated to the size of the catalyst nanoparticle. To obtain the desired diameter of SWNTs, many research groups have focused on directly controlling the size of catalyst nanoparticles using various catalyst deposition methods such as evaporations,[9,10] block copolymer micelle catalyst templates,[11−14] dendrimer-templated nanoparticles,[15] electrochemical deposition,[16] and dip-coating.[7] However, these methods have a difficulty in producing a uniform size of catalyst nanoparticles and it significantly limits their effectiveness especially toward the diameter control of SWNTs. Here we demonstrate that the diameter of SWNTs can be tailored simply by controlling the flow rate of ethanol, the carbon source for carbon nanotubes growth, in a thermal CVD process. In general, amorphous carbon produced during the CVD process coats the catalyst particles and reduces the activity and lifetime of the catalyst for CNT growth significantly. In the ethanol CVD process, controlled amounts of oxygen in the ethanol molecule (C_2H_5OH) not only work for the carbon source to grow CNTs but also serve as a weak oxidizer that would selectively remove the amorphous carbon layer on catalyst particles. In our experiment, the ethanol flow rate is controlled while maintaining all other SWNT growth parameters, such as the size distribution of the catalyst particle, temperature, pressure, and CVD process time, constant. Then, we have investigated the large-scale diameter distribution of highly dense and vertically aligned (VA) SWNTs grown with three different ethanol flow rates (50, 100, and 200 sccm) by recording Raman maps of the Radial Breathing Mode (RBM), an indicator of the SWNT diameter. In parallel with our experimental efforts, we also performed a computational investigation of the fundamental growth mechanism and growth kinetics of SWNTs under different flow rates of ethanol in the CVD process using various computational techniques, including the first-principles formalism.

Experimental Methods

The diameter controlled VA-SWNTs were synthesized by using a thermal ethanol CVD technique. In detail, a 20 nm thick Al layer was deposited onto a SiO_2 wafer as a buffer layer to grow VA-SWNTs. On top of the Al/SiO_2 layer, a 0.7−1 nm thick Co catalyst film was deposited with a sputter coater. Then the substrate was placed on a quartz tube and baked at 400 °C for 10 min in the air. After baking, the inside of the quartz tube was evacuated, and during heat-up, an argon−hydrogen mixture (5% hydrogen) was supplied as the carrier gas so that the pressure was maintained at 700 Torr. When the temperature reached at 850 °C, a controlled high-purity anhydrous ethanol

* Corresponding author. E-mail: jungy@coe.neu.edu. Phone: 1-617-373-4843. Fax: 1-617-373-2921.
[†] Northeastern University.
[‡] Kyung Hee University.
[§] HORIBA Jobin Yvon Inc.
[||] National Nanofab Center.

10.1021/jp8073877 CCC: $40.75
Published on Web 10/15/2008

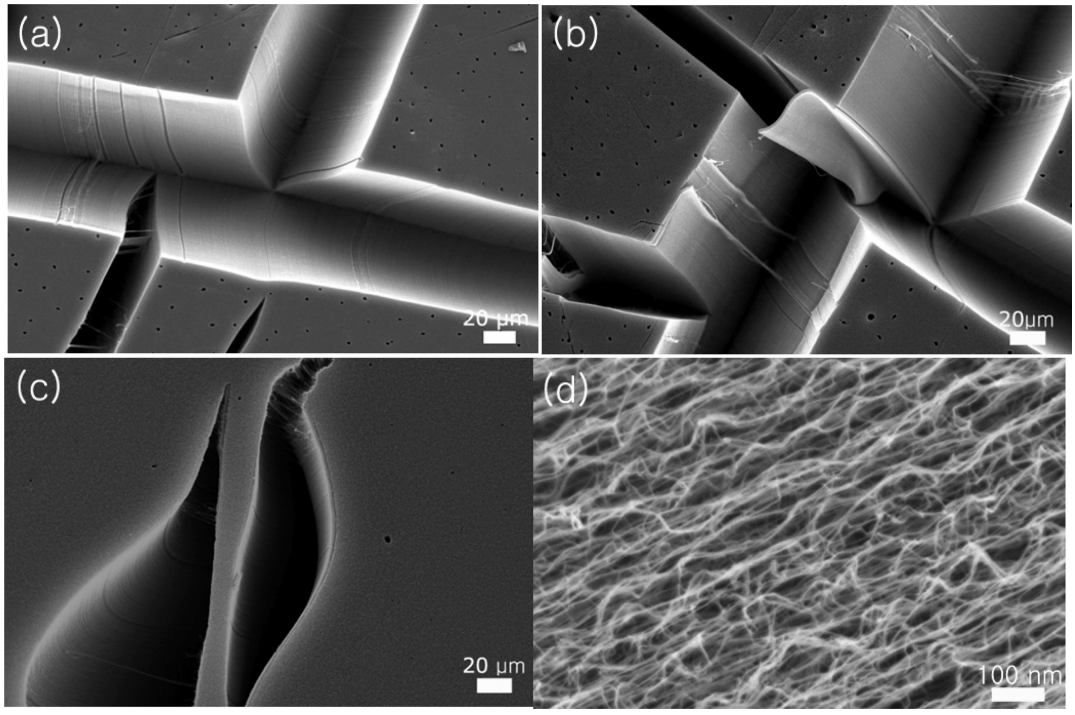

Figure 1. (a, b, c) Low-magnification SEM images of highly dense and vertically aligned SWNTs grown with 50, 100, and 200 sccm ethanol flow rate, respectively. (d) A high-magnification SEM image showing the aligned nature of SWNTs in a thermal CVD with ethanol as a carbon source.

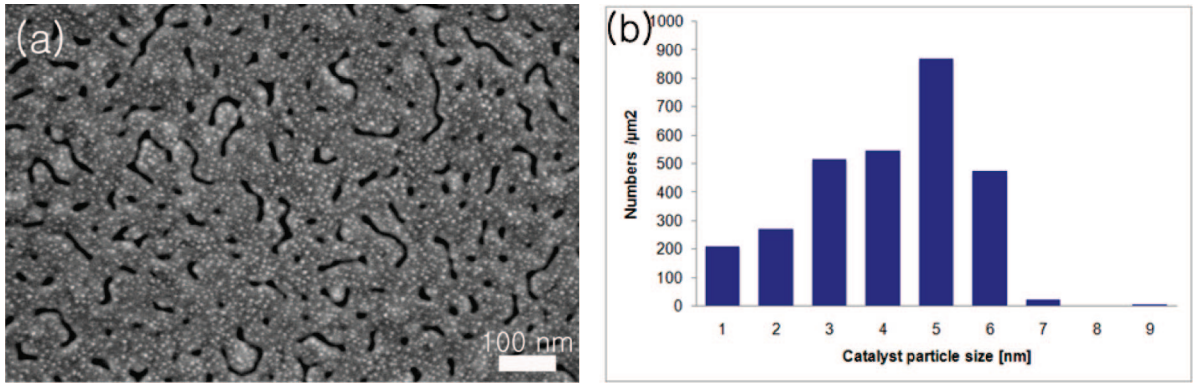

Figure 2. (a) A high-magnification SEM image showing cobalt catalyst nanoparticles on the multilayered substrate after annealing at 850 °C. (b) A histogram of catalyst particle sizes per unit area (μm^2).

(99.95%) vapor was supplied from the bubbler as a carbon source for the growth of VA-SWNTs.

Using different ethanol/argon/hydrogen mixture gas flow rates (50, 100, and 200 sccm), three different VA-SWNTs were synthesized. To investigate the large-scale diameter distribution of three different VA-SWNTs, Raman RBM maps were recorded with a Raman microscope (LabRAM HR 800, HORIBA Jobin Yvon) and a mapping stage. The Excitation laser was 785 nm, the Raman mapping area was $10 \times 10\ \mu m^2$ at 0.3 μm steps, the exposure time was 5 s/spectrum, and the number of accumulations is 14. A 600 gr/mm grating was used, and the confocal hole diameter was set to 200 μm. Raman maps were processed using the Modeling function in LabSPEC 5 (HORIBA Jobin Yvon).

Results and Discussion

Figure 1 gives typical scanning electron microscope (SEM) images of SWNTs grown using our ethanol CVD process under three different flow rates (50, 100, and 200 sccm) of ethanol. It is clearly seen that SWNTs are vertically aligned for all ethanol flow rates, 50, 100, and 200 sccm, indicating that our ethanol CVD process is very effective in growing SWNTs in high density. From TEM observation (not shown in here), we confirmed that produced CNTs were SWNTs up to 96%. The height of these VA-SWNTs is about 1 mm for growth time around 30 min and can be controlled by changing the time of the CVD process. To investigate characteristics of Co catalyst nanoparticles such as density and size distribution, after baking at 400 °C for 10 min, a thin Co catalyst film on the multilayered substrate was annealed at the temperature for SWNT growth, 850 °C for 2 min. In the high-resolution SEM image (Figure 2a), the white dots are cobalt nanoparticles and the curved black lines show the nonuniform surface morphology of the Al/SiO_2 multilayered substrate after annealing. We also observe that the size of Co catalyst nanoparticles is in the range of 1−9 nm but nanoparticle sizes with 3−6 nm are dominant in our catalyst system (Figure 2b).

The large-scale diameter distribution of VA-SWNTs grown with three different ethanol flow rates has been investigated by Raman mapping of the radial breathing mode (RBM) region

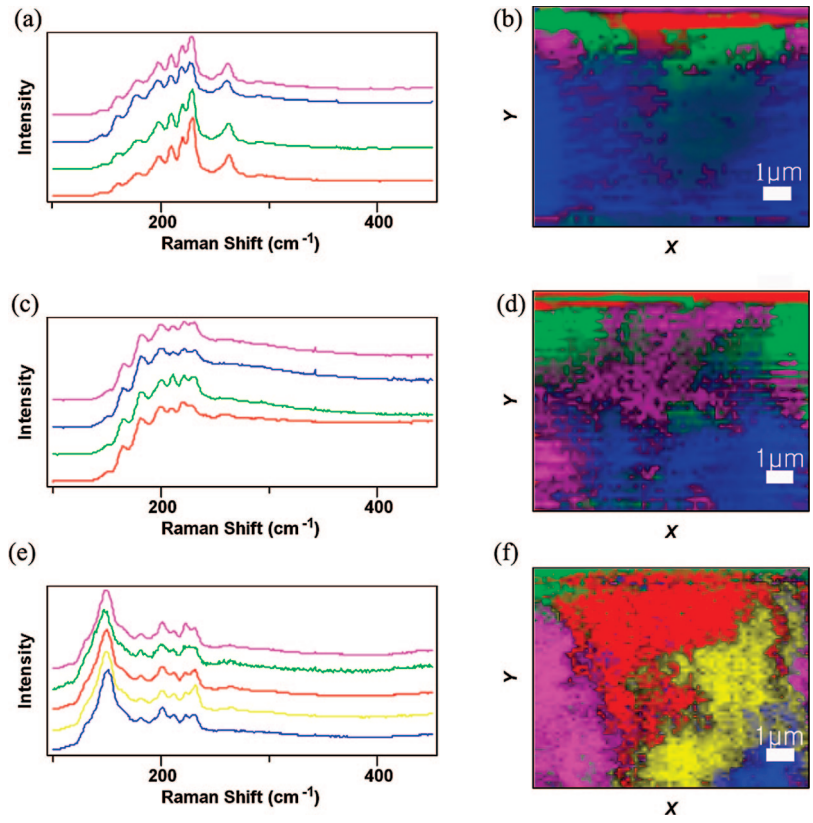

Figure 3. Raman RBM spectrum models and mapping images from vertically aligned SWNTs grown with 50 (a, b), 100 (c, d), and 200 (e, f) sccm. (a, c, e) Models produced from Raman maps of the radial breathing mode over 10 × 10 μm^2 areas at 0.3 μm steps; (b, d, f) Corresponding score images. The Raman image shows the spatial diameter distribution of SWNTs with the RBM models represented with corresponding colors

with an excitation wavelength of 785 nm. The RBM frequencies of SWNTs provide information on the diameter of SWNTs and this can be calculated from the equation d (nm) $= A/[\omega_R$ (cm^{-1}) $- 14]$, where d is the diameter of SWNT, A is the proportionality constant, and ω is the RBM frequency.[17] Several values have been reported for the proportionality constant, A, and among them, a widely used value in recent literature is 248.[18] Therefore, the diameter of SWNTs can be calculated from d (nm) $= 248/[\omega_R$ (cm^{-1}) $- 14]$. A multivariate analysis algorithm (direct classical least-squares, DCLS) was applied in an unsupervised mode to extract significantly different Raman spectra (models) and to calculate scores of individual spectra with respect to these models. RBM models and score images of three differently grown VA-SWNTs are shown in Figure 3. Raman RBM images provide the spatial distribution of SWNT diameters in the area of 10 μm × 10 μm on the surface of each sample. Subsequently, the statistical treatment of Raman RBM images can quantify the large-scale diameter distribution of VA-SWNTs. The Raman RBM map recorded from VA-SWNTs, synthesized with a 50 sccm ethanol flow rate (Figure 3a), resulted in four model spectra with the RBM peak positions ranging between 159 and 274 cm^{-1}. Each model represents a group of VA-SWNTs of the same diameter distribution. These RBM frequencies correspond to diameters of SWNT in the range of 0.90 (274 cm^{-1}) to 1.56 nm (159 cm^{-1}). The corresponding Raman RBM image shows a spatial diameter distribution of SWNTs with the four models represented with corresponding colors. For example, blue areas in the Raman RBM image represent the spatial distribution of SWNT diameters corresponding to the blue model (blue spectrum). Conversely, individual spectra from the blue area are similar to the model in blue. Vertically grown SWNTs with a 100 sccm ethanol flow rate also yielded four different RBM models whose frequencies range from 150 to 231 cm^{-1} (Figure 3c). The diameter distribution of VA-SWNTs grown with a 100 sccm ethanol flow rate is 1.07 nm (231 cm^{-1}) to 1.65 nm (150 cm^{-1}). For VA-SWNTs grown with a 200 sccm ethanol flow rate, five different RBM models in the range of 129 to 231 cm^{-1} (Figure 3e) were produced. The observed RBM frequencies correspond of SWNT diameters from 1.07 (231 cm^{-1}) to 1.92 nm (129 cm^{-1}). According to score images (Figure 3b,d,f), we could demonstrate uniformity of diameter distribution of differently grown VA-SWNTs. One model (blue model) of SWNTs grown with a 50 sccm flow rate of ethanol have a higher score up to 78% than three other models on the surface. On the other hand, for SWNTs synthesized with a 100 and 200 sccm ethanol flow rate, each model has a similar score of individual spectra on the recorded area. Therefore SWNTs grown with a 50 sccm flow rate of ethanol have uniform diameter distribution compared to SWNTs grown under a 100 and 200 sccm flow rate of ethanol.

Representative RBM spectra and a histogram of the total and major SWNT diameter distribution extracted from Raman maps of large-scale VA-SWNT films grown with three different flow rates of ethanol are shown in Figure 4. These representative RBM spectra were extracted from the RBM mapping process based on image score. It is clearly shown that, as the ethanol flow rate increases from 50 to 200 sccm, the total diameter distributions of VA-SWNTs were enlarged from 0.90−1.56 to 1.07−1.92 nm. Since the intensity of the RBM spectrum is closely correlated with the population of SWNTs on a substrate, we could also determine the major diameter distribution of VA SWNTs grown with different flow rates of ethanol by peak fitting and integrated bandwidth from each single representative RBM spectrum. As shown in Figure 4b, the major SWNT

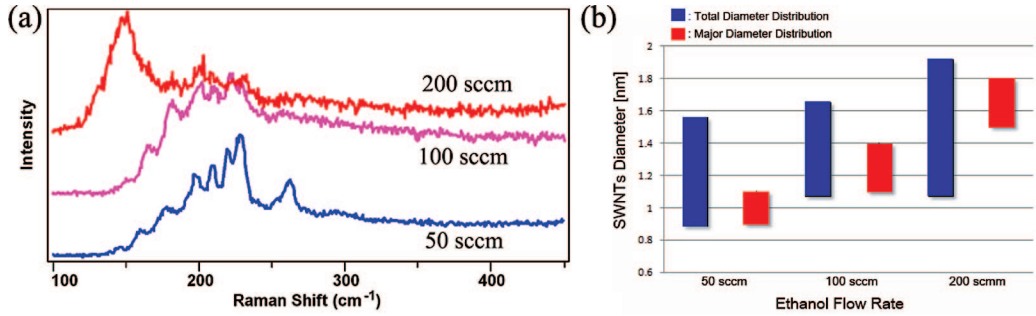

Figure 4. (a) Representative RBM spectrum of VA-SWNTs synthesized with 50, 100, and 200 sccm ethanol flow rate, respectively. (b) A histogram of the total diameter distribution and major diameter distribution of three VA-SWNTs samples.

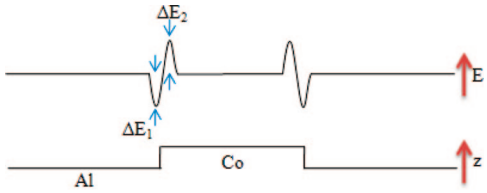

Figure 5. Schematic energy curve near the perimeter of a Co nanoparticle. ΔE_1 is the depth of attracting energy well, ΔE_2 is the height of the repelling energy barrier, and $\Delta E_1 + \Delta E_2$ is the energy barrier for captured carbon to enter the Co nanoparticle.

diameter distributions are in the range of 0.90−1.1, 1.1−1.4, and 1.5−1.8 nm for the ethanol flow rates of 50, 100, and 200 sccm, respectively, demonstrating that larger diameter SWNTs are preferentially growing as the flow rate of ethanol (carbon source) increases.

To scrutinize our experimental observation of the correlation between nanotube diameter and flow rate, we have performed the first-principle density functional theory[19−21] to calculate the diffusion barrier of carbon atoms on the surface of Co nanoparticles and Al surface, and kinetic Monte Carlo simulations to study the kinetics of carbon nanotube formation on Co nanoparticles. The calculated diffusion barrier of a carbon atom on the Co (001) surface is ~0.15 eV along the minimum barrier path, which connects the face center of a Co triangle, which is the equilibrium position, and the middle of a Co−Co bond, whereas it is ~1.5 eV through the top of a Co atom. It is expected that most carbon atoms will diffuse along the minimum barrier paths. On the Al surface, the diffusion barrier is around 0.1−0.4 eV. On the other hand, near the perimeter of the Co nanoparticle, the binding energy of a carbon atom is much higher than those on the Al surface and the Co surface. Moreover, there is a repelling barrier as shown in Figure 5. Both the binding energy and the repelling barrier become the trap energy necessary for the carbon atom to overcome in order to diffuse onto Co nanoparticles.

Different flow rates will provide different carbon flux on the substrate. Carbon source molecules are dissociated into atoms and/or smaller molecules at around 850 °C. We considered only carbon atoms that diffuse on the Al surface to study SWNT formation on the Co catalyst. While diffusing, they encounter each other to form carbon aggregations, which also diffuse, but more slowly than a single carbon atom or smaller carbon aggregations. Carbon atoms or carbon aggregations diffuse further until they meet Co nanoparticles. Since their diffusion on the Al surface is faster than their escaping ratio on the Co perimeter, they are accumulated at the perimeter of Co nanoparticles. The density of the accumulated carbon at the perimeter is determined by the carbon flux or the flow rate. As time goes on, some of the carbon atoms and aggregations at the perimeter

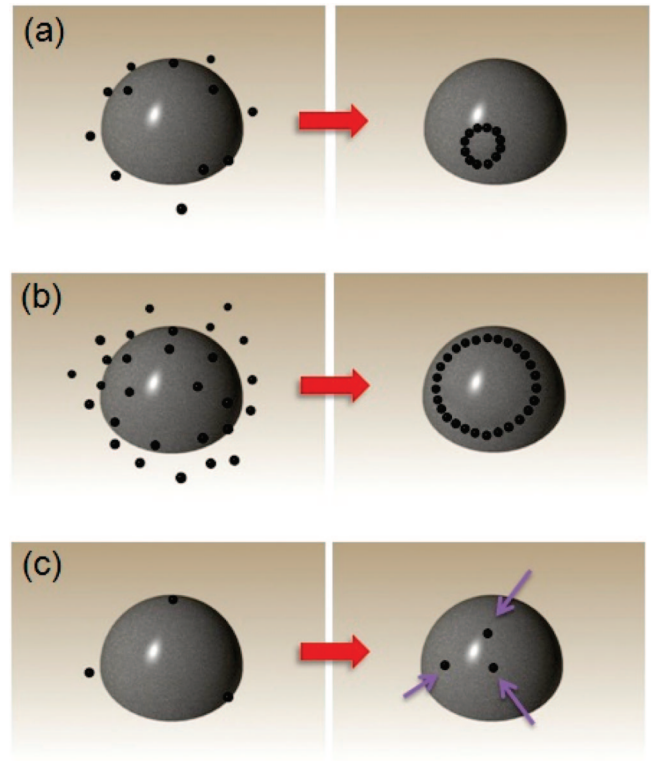

Figure 6. Schematics of our simple model for carbon nanotube growth with different flow rates: (a and b) different flow rates of carbon sources at the Co nanoparticle perimeters, which will make nucleation of carbon nanotubes with different sizes—(a) a flow rate of 50 sccm, which makes smaller diameter nanotubes and (b) a flow rate of 200 sccm, which makes larger diameter nanotubes. (c) If the flow rate is too low, then the collected carbon source at the perimeter of the Co particle is not enough to form a nucleation, so no carbon nanotube would grow.

enter onto the surface of Co nanoparticles, while some stay at the perimeter or diffuse out to the Al surface. Panels a and b of Figure 6 show schematics of different densities of carbon sources at the Co nanoparticle perimeters, which will make carbon nanotube nucleation with different sizes. Different density at the perimeter will correspond to different flow rates. For example, Figure 6a corresponds to a flow rate of 50 sccm, which makes smaller diameter nanotubes, while Figure 6b corresponds to a flow rate of 200 sccm making larger nanotubes. Figure 6c shows a situation where the flow rate is too low. In this case, the collected carbon source at the perimeter of the Co nanoparticle is not enough to form a nucleation, so no carbon nanotube would grow.

Conclusions

In conclusion, we have investigated the effect of ethanol flow rate during CVD for the diameter-controlled growth of VA-

SWNTs by using the Raman radial breathing mode (RBM) mapping process, providing large-scale spatial diameter distribution of SWNTs. SWNTs synthesized with a lower ethanol flow have a uniform diameter distribution and smaller diameter compared to that with a higher ethanol flow rate (100, 200 sccm). We have also presented a theoretical SWNT growth model under different flow rates of carbon source. From our experimental and theoretical results, it is assumed that a lower flow rate of carbon source creates a smaller nucleation site for a SWNT resulting in a smaller diameter formation. On the other hand, a higher flow rate of carbon source forms a larger nucleation site forming a SWNT with a larger diameter.

Acknowledgment. .

We acknowledge the support from the Center for High-Rate Nanomanufacturing (CHN-NSEC) at Northeastern University.

Supporting Information Available: High magnification Raman RBM spectra. This material is available free of charge via the Internet at http://pubs.acs.org.

References and Notes

(1) Graham, A. P.; Duesberg, G. S.; Seidel, R. V.; Liebau, M.; Unger, E.; Pamler, W.; Kreupl, F.; Hoenlein, W. *Small* **2005**, *1*, 382.

(2) Ngo, Q.; Cruden, B. A.; Cassell, A. M.; Sims, G.; Meyyappan, M.; Li, J.; Yang, C. Y. *Nano Lett.* **2004**, *4*, 2403.

(3) Olivier, M. K.; Oliver, G.; Christoph, E.; Louis, S. *Appl. Phys. Lett.* **1998**, *73*, 2113.

(4) Dresselhaus, M. S.; Dresselhaus, G.; Avouris, P. *Carbon Nanotubes: Synthesis, Structure, Properties, and Applications*; Springer: New York, 2001.

(5) Hata, K.; Futaba, D. N.; Mizuno, K.; Namai, T.; Yumura, M.; Iijima, S. Water-Assisted Highly Efficient Synthesis of Impurity-Free Single-Walled Carbon Nanotubes. *Science* **2004**, *306*, 1362.

(6) Maruyama, S.; Einarsson, E.; Murakami, Y.; Edamura, T. *Chem. Phys. Lett.* **2005**, *403*, 320.

(7) Murakami, Y.; Chiashi, S.; Miyauchi, Y.; Hu, M.; Ogura, M.; Okubo, T.; Maruyama, S. *Chem. Phys. Lett.* **2004**, *385*, 298.

(8) Zhang, G.; Mann, D.; Zhang, L.; Javey, A.; Li, Y.; Yenilmez, E.; Wang, Q.; McVittie, J. P.; Nishi, Y.; Gibbons, J. *PNAS* **2005**, *102*, 16141.

(9) Fan, S.; Chapline, M. G.; Franklin, N. R.; Tombler, T. W.; Cassell, A. M.; Dai, H. *Science* **1999**, *283*, 512.

(10) Javey, A.; Dai, H. *J. Am. Chem. Soc.* **2005**, *127*, 11942.

(11) Ago, H.; Ohshima, S.; Uchida, K.; Komatsu, T.; Yumura, M. *Phys. B (Amsterdam, Neth.)* **2002**, *323*, 306.

(12) Bennett, R. D.; Miller, A. C.; Kohen, N. T.; Hammond, P. T.; Irvine, D. J.; Cohen, R. E. *Macromolecules* **2005**, *38*, 10728.

(13) Fu, Q.; Huang, S.; Liu, J. *J. Phys. Chem. B* **2004**, *108*, 6124.

(14) Liu, X.; Bigioni, T. P.; Xu, Y.; Cassell, A. M.; Cruden, B. A. *J. Phys. Chem. B* **2006**, *110*, 20102.

(15) Amama, P. B.; Maschmann, M. R.; Fisher, T. S.; Sands, T. D. *J. Phys. Chem. B* **2006**, *110*, 10636.

(16) Tu, Y.; Huang, Z. P.; Wang, D. Z.; Wen, J. G.; Ren, Z. F. *Appl. Phys. Lett.* **2002**, *80*, 4018.

(17) Rao, A. M.; Chen, J.; Richter, E.; Schlecht, U.; Eklund, P. C.; Haddon, R. C.; Venkateswaran, U. D.; Kwon, Y. K.; Tomanek, D. *Phys. Rev. Lett.* **2001**, *86*, 3895.

(18) Jorio, A.; Saito, R.; Hafner, J. H.; Lieber, C. M.; Hunter, M.; McClure, T.; Dresselhaus, G.; Dresselhaus, M. S. *Phys. Rev. Lett.* **2001**, *86*, 1118.

(19) Ihm, J.; Zunger, A.; Cohen, M. L. *J. Phys. C: Solid State Phys.* **1980**, *13*, 3095.

(20) Kohn, W.; Sham, L. J. *Phys. Rev.* **1965**, *140*, A 1133.

(21) Payne, M. C.; Teter, M. P.; Allan, D. C.; Arias, T. A.; Joannopoulos, J. D. *Rev. Mod. Phys.* **1992**, *64*, 1045.

JP8073877